AFRL-SN-RS-TR-1999-76
Final Technical Report
April 1999

QUANTUM MODELING

University of Massachusetts

Gregory Sun

APPROVED FOR PUBLIC RELEASE; DISTRIBUTION UNLIMITED.

AIR FORCE RESEARCH LABORATORY
SENSORS DIRECTORATE
ROME RESEARCH SITE
ROME, NEW YORK

This report has been reviewed by the Air Force Research Laboratory, Information Directorate, Public Affairs Office (IFOIPA) and is releasable to the National Technical Information Service (NTIS). At NTIS it will be releasable to the general public, including foreign nations.

AFRL-SN-RS-TR-1999-76 has been reviewed and is approved for publication.

APPROVED: Richard A Soref

RICHARD A. SOREF
Project Engineer

FOR THE DIRECTOR: Robert V. McGahan

ROBERT V. MCGAHAN, Technical Advisor
Electromagnetics Technology Division
Sensors Directorate

If your address has changed or if you wish to be removed from the Air Force Research Laboratory Rome Research Site mailing list, or if the addressee is no longer employed by your organization, please notify AFRL/SNHC, 80 Scott Drive, Hanscom AFB, MA 01731. This will assist us in maintaining a current mailing list.

Do not return copies of this report unless contractual obligations or notices on a specific document require that it be returned.

REPORT DOCUMENTATION PAGE			Form Approved OMB No. 0704-0188

1. AGENCY USE ONLY *(Leave blank)*	2. REPORT DATE	3. REPORT TYPE AND DATES COVERED
	Apr 99	Final Aug 96 - Jul 97

4. TITLE AND SUBTITLE

QUANTUM MODELING

5. FUNDING NUMBERS

C - F30602-96-2-0199
PE - 61102F
PR - 2305
TA - DR
WU - P2

6. AUTHOR(S)

Gregory Sun

7. PERFORMING ORGANIZATION NAME(S) AND ADDRESS(ES)

University of Massachusetts
100 Morrissey Boulevard
Boston, MA 02125

8. PERFORMING ORGANIZATION REPORT NUMBER

5-28120

9. SPONSORING/MONITORING AGENCY NAME(S) AND ADDRESS(ES)

AFRL/SNHC
80 Scott Drive
Hanscom AFB, MA 01731-2909

10. SPONSORING/MONITORING AGENCY REPORT NUMBER

AFRL-SN-RS-TR-1999-76

11. SUPPLEMENTARY NOTES

AFRL Project Engineer: Richard A. Soref, SNHC, 781-377-2380

12a. DISTRIBUTION AVAILABILITY STATEMENT

Approved for public release; distribution unlimited.

12b. DISTRIBUTION CODE

13. ABSTRACT *(Maximum 200 words)*

This project analyzed the novel idea of constructing intersubband lasers on Si-based material systems, which could potentially offer the great opportunity for monolithic integration of Si-based phontonic devices with advanced Si electronics. The materials systems under investigation include quantum structures of SiGe/Si for mid- to far-infrared laser applications and of Si/ZnS for the near -infrared. The quantum-mechanical results have been published in referred journals.

14. SUBJECT TERMS

Intersubband Lasers, Phonon Scattering, Quantum Well, Superlattice, Si, SiGe, ZnS

15. NUMBER OF PAGES

36

16. PRICE CODE

17. SECURITY CLASSIFICATION OF REPORT	18. SECURITY CLASSIFICATION OF THIS PAGE	19. SECURITY CLASSIFICATION OF ABSTRACT	20. LIMITATION OF ABSTRACT
UNCLASSIFIED	UNCLASSIFIED	UNCLASSIFIED	UL

Executive Summary

The proposed research brought forth the novel idea of constructing intersubband lasers on Si-based material systems, which could potentially offer the great opportunity for monolithic integration of Si-based photonic devices with advanced Si electronics. The material systems under investigation include quantuam structures of SiGe/Si for mid- to far-infrared laser applications and of Si/ZnS for the near-infrared.

Specifically, we have studied the scattering of heavy-holes by optical phonons in SiGe/Si quantum well structures, which dominates the lifetimes of heavy-hole subbands in SiGe/Si intersubband lasers. Intrasubband and intersubband scattering rates of heavy holes are obtained due to confined nonpolar optical phonons in a $Si_{1-x}Ge_x$ quantum well with Si barriers. Guided and interface Ge-Si and Ge-Ge modes and unconfined Si-Si modes are considered. A continuum model is used for the two components of the ionic displacement of confined vibrations: the uncoupled s-polarized TO mode and the hybrid of the LO and p-polarized TO modes. The guided mode is obtained using the model of a quantum well with infinitely rigid barriers, and the interface mode is derived from the hydrodynamic boundary conditions. While the total intersubband scattering rates are reduced as a result of confinement, the opposite is found for the intrasubband scattering. Depending on the well width and Ge content, the intersubband scattering rates are reduced by a factor of two to four with respect to their values for no confinement. Thus, one would expect comparable enhancement in the intersubband lifetimes crucial to the population inversion in a $Si_{1-x}Ge_x$/Si intersubband laser.

We have also calculated the valence subband engeries and wavefunctions in Si/ZnS quantum well structures. We have also established models for the confined optical phonons in Si/ZnS superlattices. Optical phonon modes in Si and ZnS layers are totally confined within their respective layers since both layers can be treated as infinitely rigid with respect to the other layer. Since there are no associated electric fields with nonpolar optical phonons in Si layers, only a mechanical boundary condition needs to be satisfied for these nonpolar optical modes at the Si-ZnS interface. The optical phonons in Si layers can be described by guided modes consisting of an uncoupled s-TO mode and a hybrid of LO and p-TO modes with no interface modes. In ZnS layers, a continuum model hybridizing the LO, TO and IP modes is necessary to satisfy both the mechanical and electrostatic boundary conditions at the heterointerface. A numerical procedure is provided to determine the common frequency between LO, TO, and IP modes. This is a new procedure for obtaining the eigen modes of a mixed polar-nonpolar heterosystem. Analytical expressions are obtained for the ionic displacement and associated electric field as well as scalar and vector potentials. The established model can be used to calculate the phonon scattering process of carriers in Si/ZnS heterostructures and ultimately provide a theoretical basis for studying the Si/ZnS intersubband lasers.

Part I. A study of confined nonpolar optical phonons and their interaction with carriers in SiGe/Si quantum well structures

I. INTRODUCTION

The possibility of lasing due to intersubband transitions in quantum well (QW) structures is crucially dependent on the lifetimes of the involved subbands. In an earlier communication[1] lifetimes were calculated for a $Si_{1-x}Ge_x$/Si multiple quantum well (MQW) structure due to acoustic and nonpolar optical phonon scattering. It was pointed out that, because of the absence of polar optical scattering for silicon-based systems, the lifetimes and their differences are consistently an order of magnitude larger than for the GaAs/AlGaAs system, and do not show the marked decrease when the intersubband energy exceeds the optical phonon energy. For this case, the scattering was calculated for propagating phonons corresponding to the average composition, assuming no confinement. As pointed out in that paper, it is expected that this treatment of phonon scattering leads to an overestimate of the intersubband transition rates, and therefore provides a conservative approach in determining the subband lifetimes. In order to more accurately determine the subband lifetimes, it is necessary to take into account confinement effects on optical phonons in heterostructures. In a $Si_{1-x}Ge_x$/Si QW structure, one can expect Si-Si, Ge-Si, and Ge-Ge optical modes in the alloy.[2] The Ge-Si and Ge-Ge modes tend to be confined by the Si barriers as has been seen in Raman scattering experiments.[3] The phonon confinement gives rise to guided and interface modes which will scatter the carrier less for intersubband transitions, thus resulting in revised subband lifetimes. This is due to the discrete spectrum of the guided modes and the weak intersubband scattering of interface modes. However, the intrasubband scattering process tends to be enhanced due to confinement.

There has been a great deal of effort in dealing with the issue of phonon confinement in heterostructures.[2]-[21] Most of published literature have focused on confined polar optical phonons, because a large body of the heterostructures are constructed from polar semiconductor materials. Recently, the demonstration of an infrared intersubband transition laser in the InGaAs/AlGaAs material system[22] has renewed interest in investigating the possibility of constructing lasers within the Ge/Si material system, which eventually would allow monolithic integration of optical components with advanced Si microelectronics.

A self-consistent continuum theory of confined nonpolar optical phonons has been developed for an infinite plate with free boundary conditions.[4] In the present paper, we extend that continuum theory to examine the confined nonpolar optical phonons of Ge-Si and Ge-Ge vibration modes with proper mechanical boundary conditions in a $Si_{1-x}Ge_x$/Si QW. Furthermore, we use these results to estimate the heavy-hole scattering rates by the nonpolar optical phonons. To the best of our knowledge, there has not been any work in estimating the scattering rates due to the nonpolar optical phonons in $Si_{1-x}Ge_x$/Si heterostructures taking into account phonon confinement.

The three different vibration modes, namely, Si-Si, Ge-Si, and Ge-Ge, are considered separately and are given proper weights in heavy-hole scattering calculation. The Si-Si mode propagates freely throughout the structure, while the Ge-Si and Ge-Ge modes are confined by the barriers, resulting in guided and interface modes. Approximations made in the course of the calculations for the guided and interface modes will be discussed. We will examine both intrasubband and intersuband scattering processes. We will also compare these results with those assuming no confinement. We will show that indeed the latter assumption overestimates the scattering rates for intersubband transitions, but tends to underestimate the intrasubband process. The difference is largely attributed to the heavy-hole interaction with interface modes which can be neglected for the intersubband process, but contributes significantly to the intrasubband process. The scattering rates due to various scattering modes will be investigated as a function of the well width and as a function of the alloy composition of the well.

II. PHONON CONFINEMENT

Phonon confinement occurs due to the lack of overlap of the bulk frequency dispersions in the adjacent heterostructure materials. Thus in a Si/Ge/Si short period superlattice, the higher frequency optical modes of Si correspond to an frequency gap in the Ge layer and are therefore confined. The Ge modes in the Ge layers are strictly resonant with the Si acoustic modes and are 'quasi-confined', but the displacement pattern is similar to that of a true confined mode and indeed the Raman intensities are comparable.[2] The Raman spectrum has revealed that there exist Ge-Ge, Ge-Si, and Si-Si vibration modes in the $Si_{1-x}Ge_x$ alloy layer.[3] The Ge-Ge vibrations have phonon energy of $37.4meV$ and the Ge-Si vibrations of $50.8meV$. These two modes of the $Si_{1-x}Ge_x$ well are confined by the Si-Si modes of the barrier (phonon energy $64.3meV$); however, the Si-Si optical modes of the well are unconfined, as are the Si-Si optical modes of the barrier.

One of the simplest conceptual model is to treat the QW system with infinitely rigid barrier. The boundary condition to be satisfied is the vanishing of the ionic displacement of all confined vibration modes. This is an assumption of strict confinement, yielding guided modes of the confined phonons. This assumption needs to be partially relaxed in order to admit interface modes. As pointed out in the continuum theory,[4] the ionic displacement of confined vibrations has two components: one is the hybrid of the LO and p-polarized TO (p-TO) modes, and the other is the uncoupled s-polarized TO (s-TO) mode. These modes are defined as follows: if we consider a (x, z) plane containing the normal to the layers and the phonon wavevector $\mathbf{Q}$, then

$$\mathbf{Q} = q_x \hat{e_x} + q_z \hat{e_z} \tag{1}$$

where $\hat{e_x}$ and $\hat{e_z}$ are unit vectors. The p-TO mode has its displacements normal to $\mathbf{Q}$ and in the (x, z) plane, while the s-TO displacements are normal to $\mathbf{Q}$ and perpendicular to the (x, z) plane ($||\hat{e_y}$). A description of the s-TO mode is

$$u_y = e^{iq_x x}(Ae^{iq_z z} + Be^{-iq_z z}), \tag{2}$$

while the hybrid of the LO and p-TO modes is given by

$$\begin{aligned} u_x &= e^{iq_x x}[q_x(Ce^{iq_L z} + De^{-iq_L z}) + q_T(Ee^{iq_T z} + Fe^{-iq_T z})], \\ u_z &= e^{iq_x x}[q_L(Ce^{iq_L z} - De^{-iq_L z}) - q_x(Ee^{iq_T z} - Fe^{-iq_T z})]. \end{aligned} \tag{3}$$

The z-components of the LO and TO wavevector have been distinguished by q_L and q_T, respectively.

The above choice for the ionic displacement guarantees that

$$\nabla \times \mathbf{u}_L = 0 \quad \text{and} \quad \nabla \cdot \mathbf{u}_T = 0, \tag{4}$$

which hold for isotropic materials (assumed here), allowing $\mathbf{u}$ to be decomposed into LO and TO components,

$$\mathbf{u} = \mathbf{u}_L + \mathbf{u}_T. \tag{5}$$

Since the LO and TO modes must have the same frequency to be effectively coupled, they have to satisfy, according to the bulk LO and TO dispersions,

$$\omega^2 = \omega_0^2 - \beta_L^2(q_x^2 + q_L^2) = \omega_0^2 - \beta_T^2(q_x^2 + q_T^2), \tag{6}$$

where β_L and β_T are the velocities of LO and TO dispersions, respectively.

Guided Modes

In the case of strict confinement, the boundary condition of course is that the displacements $\mathbf{u}$ vanish at the boundaries $z = (0, L)$. For the s-TO mode, this leads to

$$u_y = Ae^{iq_x x}\sin(q_z z), \qquad \text{with} \quad q_z = \frac{n\pi}{L} \tag{7}$$

where $n = 1, 2, \cdots$. This mode does not mix with other modes, nor does it give rise to the interface mode discussed later. The s-TO mode pattern for $q_z = \pi/L$ is shown in Fig.1(a) with the well width $L = 40\mathring{A}$.

For the coupled LO and p-TO modes, applying the boundary conditions of $u_x = 0$ and $u_z = 0$ at $z = (0, L)$ to Eq.(3) leads to a system of four constant-coefficient linear equations for C, D, E, and F. The vanishing of the determinant of the 4×4 constant coefficient matrix gives rise to the following relation,

$$(q_T q_L + q_x^2)^2 \sin(q_T L)\sin(q_L L) = 2q_T q_L q_x^2[\cos(q_T - q_L)L - 1]. \tag{8}$$

Eq.(8) leads to solutions of guided modes consisting of coupled phase-matched LO and TO modes with wavevectors

$$q_L = \frac{n_L\pi}{L} \quad \text{and} \quad q_T = \frac{n_T\pi}{L}, \tag{9}$$

where $n_L = 1, 2, \cdots$, $n_T = 3, 4, \cdots$, and $n_T - n_L = 2, 4, 6, \cdots$. This choice of quantum numbers is due to the constraint Eq.(6) since $\beta_T < \beta_L$.

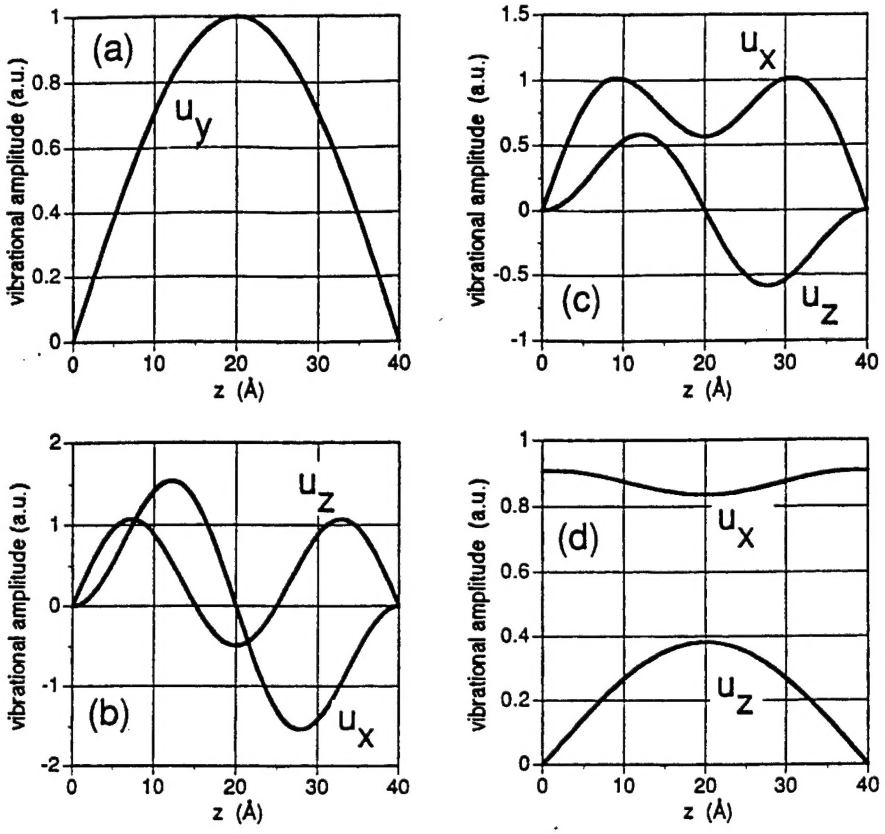

Figure 1. Vibration patterns for (a) the guided s-TO mode, (b) the 'sine' solution, (c) the 'cosine' solution of the guided p-TO and LO modes, and (d) the coupled p-TO and LO interface mode for the well width of 40Å.

Two sets of guided mode solutions emerge and they are given in either sine or cosine form referring to the z-component of the ionic displacement. The 'sine' solution is

$$\begin{aligned} u_x &= 2Ce^{iq_x x} q_x [\cos(q_L z) - \cos(q_T z)], \\ u_z &= 2iCe^{iq_x x} [q_L \sin(q_L z) + \frac{q_x^2}{q_T} \sin(q_T z)], \end{aligned} \tag{10}$$

and a 'cosine' solution

$$\begin{aligned} u_x &= 2iCe^{iq_x x} [q_x \sin(q_L z) + \frac{q_L q_T}{q_x} \sin(q_T z)], \\ u_z &= 2Ce^{iq_x x} q_L [\cos(q_L z) - \cos(q_T z)]. \end{aligned} \tag{11}$$

The hybrid patterns of the p-TO and LO modes with $q_L = \pi/L, q_T = 3\pi/L$ are shown in Fig.1(b,c) for the 'sine' and 'cosine' solutions, respectively, with the well width $L = 40\text{Å}$.

It is worthwhile to point out the similarities between the allowed values of q_z, q_L, q_T and q_x for the guided modes in the case of infinitely rigid barriers assumed here and that of an infinite plate with free boundary conditions.[4] But the displacement patterns differ dramatically between the two situations.

As pointed out by Mori and Ando[13], Nash[14], and Register[15], a sum rule can be derived for polar optical scattering relating the form factors of the confined modes to that of the 'bulk' modes. Such a sum rule, as pointed out by Nash[14], arises from the completeness and orthogonality of the vibration sets. As derived, this applies to polar optical scattering accompanied by a macroscopic electrical potential. As is well known, the latter removes the degeneracy of the zone center optical phonons and the carrier interacts only with the LO mode. However, for the nonpolar optical phonons of interest in the present work, both TO and LO modes interact with the carrier. As discussed earlier, the s-TO mode does not mix with the other modes and can be described in terms of an orthogonal and complete set of functions given by Eq.(7). However, the p-TO and LO modes are coupled as given by Eqs.(10) and (11), with the constraint given by Eq.(6) that the frequencies be equal, taking account of the different frequency dispersions. The LO and p-TO cannot be treated independently because, having chosen their forms to satisfy Eq.(4), the vanishing boundary boundary conditions at $z = 0$ and $z = L$ cannot be satisfied for $\mathbf{u}_L$ and $\mathbf{u}_T$ independently. As a consequence of the coupling, in satisfying the boundary conditions for the guided modes, not all values of wavevectors (q_x, q_L, q_T) are allowed and so the set is not complete. Specifically, the allowed values of (q_L, q_T) require that q_x be discrete, not continuous, and be given by

$$q_x^2 = (\frac{\pi}{L})^2 \frac{\beta_T^2 n_T^2 - \beta_L^2 n_L^2}{\beta_L^2 - \beta_T^2}, \tag{12}$$

where n_L and n_T have been defined in Eq.(9). Further, two modes which differ in only one of (q_L, q_T) are not orthogonal. In summary, in comparison with the guided modes for polar optical phonons, even though the guided modes constitute a complete orthogonal set for the s-TO modes in the y-direction, the linear combination of p-TO and LO modes in the (x, z) plane are neither complete nor orthogonal. Hence, a sum rule cannot be applied to the current basis set for nonpolar optical phonons.

Interface Modes

The assumption of strict confinement, that the vibration amplitudes are zero at the interfaces, rules out the possibility of interface modes. In general such modes exist and are of increasing importance in carrier scattering intrasubband transitions in comparison with guided modes. The assumption of strict confinement must therefore be relaxed to admit such modes. It is obvious that the amplitudes of interface modes at the boundaries should remain small in order to keep the assumption of strict confinement yielding the guided modes. In fact, we need only to relax the vanishing assumption of the x-component of the displacement to admit interface modes while maintaining the zero boundary condition on the z-component. A similar boundary condition has been employed in treating the polar optical phonons for a single GaAs/AlAs QW.[10]

Applying the hydrodynamic boundary conditions[5] at the interfaces to the LO and TO modes independently and considering the fact that the optical phonon frequency in the barrier region is greater than that in the well region, we obtain only a solution with even z-component for the LO mode,

$$\mathbf{u}_L = \begin{cases} Ce^{iq_x x}(q_x\hat{e}_x - q_{L2}\hat{e}_z)e^{-iq_{L2}z} & z < 0, \\ Ce^{iq_x x}(\frac{\rho_1}{\rho_2})^{1/2}(\frac{\eta_2}{\eta_1}\frac{\rho_2}{\rho_1}q_x\hat{e}_x - q_{L2}\hat{e}_z) & 0 < z < L, \\ -Ce^{iq_x x}(q_x\hat{e}_x + q_{L2}\hat{e}_z)e^{iq_{L2}(z-L)} & z > L, \end{cases} \tag{13}$$

where the subscripts 1 and 2 refer to well ($Si_{1-x}Ge_x$) and barrier (Si) regions, respectively, ρ_i is the material density, and

$$\eta_i = \omega_i^2/\omega^2 - 1, \tag{14}$$

where ω_i is the Γ-point optical phonon frequency in layer i $(= 1, 2)$. For both Ge-Si and Ge-Ge confined modes we have $\omega_2 > \omega_1$. The LO wavevector in the well region $q_{L1} = 0$ and that in the barrier region,

$$q_{L2}^2 = \frac{\omega_2^2 - \omega_1^2}{\beta_2^2} + (\frac{\beta_1^2}{\beta_2^2} - 1)q_x^2 \tag{15}$$

The LO mode solution is of two-dimensional bulk type with constant amplitudes in the well region propagating with wavevectors parallel to the interfaces.

Both odd and even solutions emerge for the TO mode, but the boundary condition that the z-component of $\mathbf{u}_L + \mathbf{u}_T$ vanishes at the interfaces admits only the even solution,

$$\mathbf{u}_T = \begin{cases} De^{iq_x x}(q_{T2}\hat{e}_x + q_x\hat{e}_z)e^{-iq_{T2}z} & z < 0, \\ De^{iq_x x}(\frac{\rho_1}{\rho_2})^{1/2}\dfrac{1}{\cos(q_{T1}L/2)} & \\ \quad \times [-iq_{T1}\sin q_{T1}(z - L/2)\hat{e}_x + q_x\cos q_{T1}(z - L/2)\hat{e}_z] & 0 < z < L, \\ -De^{iq_x x}(q_{T2}\hat{e}_x - q_x\hat{e}_z)e^{iq_{T2}(z-L)} & z > L, \end{cases} \tag{16}$$

where the wavevectors for the TO mode, according to Eq.(6) .

$$\begin{aligned} q_{T1}^2 &= (\frac{\beta_{L1}^2}{\beta_{T1}^2} - 1)q_x^2 && \text{(well)}, \\ q_{T2}^2 &= (\frac{\beta_{L2}^2}{\beta_{T2}^2} - 1)q_x^2 + \frac{\beta_{L2}^2}{\beta_{T2}^2}q_{L2}^2 && \text{(barrier)}. \end{aligned} \tag{17}$$

Combining Eqs.(13) and (16) and applying that the z-component of $\mathbf{u}_L + \mathbf{u}_T$ vanishes

at the interfaces, lead to $D = (q_{L2}/q_x)C$, and finally the interface mode is obtained,

$$\mathbf{u} = \begin{cases} Ce^{iq_x x}[(q_x e^{-iq_{L2}z} + \dfrac{q_{L2}q_{T2}}{q_x} e^{-iq_{T2}z})\hat{e_x} \\ \qquad + (-q_{L2}e^{-iq_{L2}z} + q_{L2}e^{-iq_{T2}z})\hat{e_z}] & z < 0, \\ Ce^{iq_x x}(\dfrac{\rho_1}{\rho_2})^{1/2}\{[\dfrac{\eta_2}{\eta_1}\dfrac{\rho_2}{\rho_1}q_x - \dfrac{i}{\cos(q_{T1}L/2)}\dfrac{q_{L2}q_{T1}}{q_x}\sin q_{T1}(z - L/2)]\hat{e_x} \\ \qquad + q_{L2}[\dfrac{\cos q_{T1}(z - L/2)}{\cos(q_{T1}L/2)} - 1]\hat{e_z}\} & 0 < z < L, \\ Ce^{iq_x x}\{[-q_x e^{iq_{L2}(z-L)} - \dfrac{q_{L2}q_{T2}}{q_x}e^{iq_{T2}(z-L)}]\hat{e_x} \\ \qquad + [-q_{L2}e^{iq_{L2}(z-L)} + q_{L2}e^{iq_{T2}(z-L)}]\hat{e_z}\} & z > L. \end{cases} \tag{18}$$

Fig.1(d) shows the pattern of an interface mode in the well region responsible for the scattering process from subband 2 to 1 by emitting a Ge-Si optical phonon with $L = 40\mathring{A}$. It can be seen from Fig.1(d) that the x-component of the displacement is approximately constant within the well region and the z-component vanishes at both interfaces.

The above form of the interface mode derived from the hydrodynamic boundary conditions is different from that of the surface mode for the infinite free plate[4] and that for the interface mode for polar materials. The difference from the former case arises from the different boundary conditions since the free surface requires that the dilation stress perpendicular to the surface and the shear stress across the surface vanish. The difference from the latter is primarily due to the fact that the zone-center optical phonon frequency in the barriers is greater than that in the well, which is contrary to the situation in GaAs/AlGaAs material systems.

The dispersion of bulk Si-Si mode has little overlap with that of Ge-Si mode. The scattering process involves only long wavelength in-plane wavevectors, and the z-components of phonon wavevectors in the barriers, q_{L2} and q_{T2}, are approximately the dimension of the Brillouin zone. This is because the dispersion relations overlap only at large phonon wavevectors in the barrier region. Since $q_{L1} = 0$ and $q_x \approx 0$, the interface mode frequency $\omega \approx \omega_1$, therefore, $\eta_2/\eta_1 >> 1$. The major scattering contribution from the interface mode is from the displacement in the well region where the heavy-holes are confined. The amplitude of the LO-component is much greater than that of the TO-component in Eq.(18) for $0 < z < L$, since

$$\frac{\eta_2}{\eta_1}\frac{\rho_2}{\rho_1} >> \frac{q_{L2}q_{T1}}{q_x^2} \tag{19}$$

considering q_{T1} also small. Therefore, the exact values of q_{L2} and q_{T2} are not crucial in determining the scattering rates because the TO mode contribution is at least two orders of magnitude less than the LO mode. The above displacement pattern Eq.(18) has been used in evaluating the interface mode scattering for the confined Ge-Si and Ge-Ge modes.

III. HEAVY HOLE SCATTERING RATES

The nonpolar optical phonon interaction Hamiltonian involving a heavy hole is[23]

$$H = \frac{(M_1 M_2)^{1/2}}{M_1 + M_2} \mathbf{D} \cdot \mathbf{u} \tag{20}$$

where M_1 and M_2 are the masses of the two atoms in the unit cell, and $\mathbf{D}$ is the optical deformation potential.

The normalization of the displacement amplitudes is carried out through the approach of equating the energy of the vibration mode with that of a simple harmonic oscillator[9] as

$$\chi^2 = \frac{S}{\Omega} \int_0^L \mathbf{u}^* \cdot \mathbf{u} dz, \tag{21}$$

where L is the well width, S is the sample surface area (in (x, y) plane), Ω is the volume of the unit cell, and χ is the normal coordinator of the oscillator.

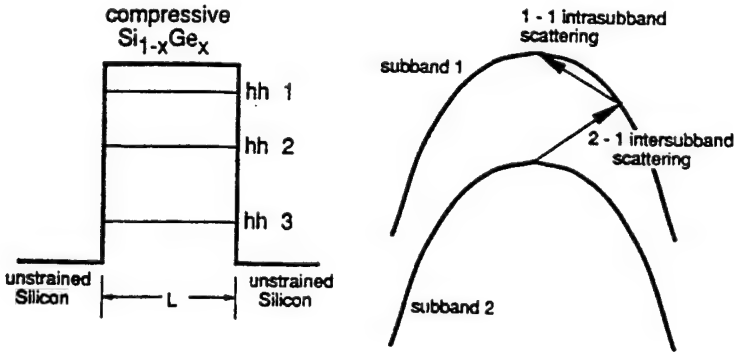

Figure 2. Heavy hole band structure and scattering processes.

The heavy-hole band offset is calculated taking into account the compressive strain in the $Si_{1-x}Ge_x$ well region.[24] The heavy-hole bands are decoupled from the light-hole and split-off bands at $\mathbf{k} = 0$ and can be treated independently.[25] The heavy-hole energy levels and envelope wavefunctions are obtained by the finite square well model as shown in Fig.2. The heavy-hole state can be characterized by $|\mathbf{k}, n>$ with the in-plane momentum $\mathbf{k}$ and subband index n. In the approximation of constant effective mass for heavy holes, the matrix element for the transition from state $|\mathbf{k}, n>$ to $|\mathbf{k}', n'>$

due to nonpolar optical phonon scattering is

$$< \mathbf{k}', n'|H|\mathbf{k}, n >= \begin{cases} \sqrt{\dfrac{\hbar[n(\omega_o)+1/2\mp 1/2]}{2\rho_1\omega_o SL\Delta_A(q_z)}}\delta_{\mathbf{k}'\pm\mathbf{q}_x,\mathbf{k}} D_y G^y_{nn'}(q_z) & \text{(s-TO)} \\ \sqrt{\dfrac{\hbar[n(\omega_o)+1/2\mp 1/2]}{2\rho_1\omega_o SL\Delta_C(q_L,q_T)}}\delta_{\mathbf{k}'\pm\mathbf{q}_x,\mathbf{k}} & \\ \quad \cdot [D_x G^x_{nn'}(q_L,q_T) + D_z G^z_{nn'}(q_L,q_T)] & \text{(hybrid)}, \end{cases} \tag{22}$$

for the s-TO mode and the hybrid of the LO and p-TO mode, respectively. $n(\omega_o)$ is the number of optical phonons at thermal equilibrium, and the upper and lower signs refer to phonon absorption and emission, respectively. The three components of the optical deformation potential, D_x, D_y, and D_z are assumed equal to $D_o = D/\sqrt{3}$ in the calculation, in view of the assumption of isotropy. The Kronecker symbol indicates the in-plane (x, y) momentum conservation. The normalization factors are given by

$$\begin{aligned} \Delta_A(q_z) &= \frac{1}{L}\int_0^L u_y^* u_y dz \qquad && \text{(s-TO)}, \\ \Delta_C(q_L,q_T) &= \frac{1}{L}\int_0^L (u_x^* u_x + u_z^* u_z) dz \qquad && \text{(hybrid)}. \end{aligned} \tag{23}$$

The $G_{nn'}$-functions contain envelope wavefunctions, ψ_n and ψ'_n, from which interference effect can be obtained. Specifically,

$$G^y_{nn'}(q_z) = \int_0^L \psi_n \psi_{n'} u_y dz, \tag{24}$$

for the s-TO mode, and

$$\begin{aligned} G^x_{nn'}(q_L,q_T) &= \int_0^L \psi_n \psi_{n'} u_x dz, \\ G^z_{nn'}(q_L,q_T) &= \int_0^L \psi_n \psi_{n'} u_z dz, \end{aligned} \tag{25}$$

for the hybrid of LO and p-TO mode. It should be noted that given the proper displacement expressions, Eq.(22) for the matrix element is valid for both the guided and interface modes discussed above.

Obviously, depending on the alloy composition in the well, the three modes (Si-Si, Ge-Si, and Ge-Ge) will have different interaction strengths with the carriers in the QW structure. Specifically, each interaction should be weaker than that for the case where it is the only existing mode and therefore needs to be accounted for properly. A crude model to approximate the relative strength of each individual mode is to assign a weight in the calculation of the phonon scattering rate. If we assume bonds formed between Si-Si, Ge-Si, and Ge-Ge are purely random, then we can give the following weights according to the Ge content, x, to each of the vibration modes in the $Si_{1-x}Ge_x$ well: $w_{Si} = (1-x)^2$ for Si-Si mode, $w_{GeSi} = 2x(1-x)$ for Ge-Si mode, and $w_{Ge} = x^2$ for Ge-Ge mode.

Applying the Fermi golden rule, we obtain the scattering rate due to the guided modes,

$$W^j_{nn'} = \begin{cases} \frac{w_j m^*_{hh}[n(\omega_o)+1/2\mp 1/2]D_o^2}{2\hbar^2\rho_1\omega_o L}\sum_{q_z}\frac{|G^y_{nn'}|^2}{\Delta_A} & \text{(s-TO)} \\ \frac{w_j m^*_{hh}[n(\omega_o)+1/2\mp 1/2]D_o^2}{2\hbar^2\rho_1\omega_o L}\sum_{q_L,q_T}\frac{|G^x_{nn'}+G^z_{nn'}|^2}{\Delta_C} & \text{(hybrid)}, \end{cases} \tag{26}$$

where we have assumed that for the intersubband process ($n \neq n'$) the heavy holes are scattered from the bottom of their original subbands, and for the intrasubband process ($n = n'$) the heavy holes have just enough kinetic energy (equal to the Si-Si optical phonon energy) to emit an optical phonon to reach to the bottom of the same subband. w_j (j =Ge-Si, Ge-Ge) is the weight assigned to a particular vibration mode and m^*_{hh} is the heavy-hole effective mass.

For the s-TO guided mode, the summation in Eq.(26) is over all $q_z = n\pi/L$ limited by

$$q_z^2 < (\frac{\pi}{a_j})^2 - q_x^2, \tag{27}$$

where a_j is the lattice constant and q_x is given by the constraint of the in-plane momentum conservation. For the hybrid guided mode, the summation is restricted to those combinations of $q_L = n_L\pi/L$ and $q_T = n_T\pi/L$ which, according to Eq.(6), yield discrete values of q_x satisfying the in-plane momentum conservation. It should be pointed out that an unique final state heavy-hole wavevector $\mathbf{k}'$ (initial $\mathbf{k} = \mathbf{0}$) will result if the phonon frequency dispersion is neglected, corresponding to a constant optical phonon energy. Then the in-plane momentum conservation would be impossible since the discrete values of q_x will not be able to exactly match the unique value of $\mathbf{k}'$. However, taking into account of the phonon dispersion, a region of heavy-hole wavevector $\mathbf{k}'$ will be obtained and the scattering process is permitted as long as q_x lies in that region.

There is no s-TO interface mode, and the scattering rate due to the hybrid interface mode can be given, similarly,

$$W^j_{nn'} = \frac{w_j m^*_{hh}[n(\omega_o)+1/2\mp 1/2]D_o^2}{2\hbar^2\rho_1\omega_o L\Delta_C}|G^x_{nn'}+G^z_{nn'}|^2, \tag{28}$$

where $G^x_{nn'}$ and $G^z_{nn'}$ are functions of q_{T1}, q_{L2}, and q_{T2} with $q_{L1} = 0$. The determination of the phonon wavevectors in the well and barrier regions have been discussed in section II. Eqs.(26) and (28) are used to evaluate both the intrasubband and intersubband transitions due to the confined phonons of Ge-Si and Ge-Ge modes. However, since the Si-Si vibration is unconfined, the calculation of its scattering rate is trivial.[26]

Intrasubband Scattering

The intrasubband scattering rate was calculated assuming that the transition originated from the heavy-hole state with a kinetic energy equal to the Si phonon energy

to the bottom of the same subband. Therefore, only the process of phonon emission is considered in the calculation. All results are obtained at room temperature. The structure parameters are varied within the limits for producing metastable strained $Si_{1-x}Ge_x$ alloy on the Si substrate.[27] Fig.3 shows the intrasubband transition rates (1-1) within the ground-state heavy-hole subband ($n = 1$) due to the Ge-Si and Ge-Ge guided and interface modes as a function of the well width for a $Si_{0.5}Ge_{0.5}$/Si QW. It can be seen that for the intrasubband process the strength of interface mode scattering is about same order of magnitude as that of corresponding guided mode. This is in contrast with the intersubband process discussed later. The scattering rates of both guided and interface modes for Ge-Si and Ge-Ge vibrations increases with the increase of the well width when it is narrow ($L < 25\mathring{A}$). This is due to the increase of the interference G-function with $n = n' = 1$ given in Eqs.(24) and (25) as the envelope function for subband 1 becomes more confined in the well region for larger well width. However, the G-function increase becomes negligible as the well width increases further since the envelope function has mostly been confined within well region. Examining the interface scattering rate given in Eq.(28), one would expect it to decrease with the further increase of the well width, which is clearly demonstrated in Fig.3 for both Ge-Si and Ge-Ge phonon interactions. A similar decrease of the interface scattering rate in a GaAs/Al_xGa_{1-x}As QW has been reported.[7]

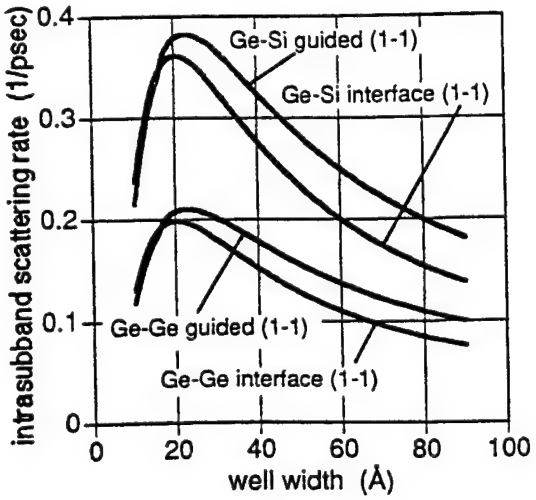

Figure 3. Intrasubband scattering rates in the lowest subband ($n = 1$) due to Ge-Si and Ge-Ge guided and interface modes as a function of well width with $x = 0.5$.

For the guided mode, the scattering rate is given by summing the contributions from the s-TO and hybrid of LO and p-TO modes. However, the hybrid interaction with the heavy holes is much weaker than the s-TO mode, because of the requirements on the hybrid mode to simultaneously satisfy the in-plane momentum conservation and the frequency dispersion Eq.(6). This excludes the interaction of most hybrid modes

with the heavy holes, leaving the s-TO modes as the dominant scattering mechanism. In fact, the number of allowed s-TO vibration modes will increase with the increase of the well width. It is easy to see from Eq.(24) that for the intrasubband process ($n = n'$) the interference G-function is nonzero only for even s-TO modes ($n_{q_z} = 1, 3, 5, \cdots$), and the largest contribution is from the lowest order mode $n_{q_z} = 1$ with higher order modes being at least two orders of magnitude less. The guided mode scattering for the intrasubband process is therefore practically a single s-TO mode interaction and behaves similarly to the interface mode. The difference between the Ge-Si and Ge-Ge vibrations is mainly due to the different weights assigned to them according to the Ge content in the Si_xGe_{1-x} alloy. Our calculation also showed that the (2-2) intrasubband scattering process has very similar behavior as the interface mode scattering and has a slightly higher scattering rate than the guided mode, but overall smaller rates compared to the (1-1) process.

Fig.4(a) shows the total scattering rate as a function of the well width, which is given by summing the contributions from the Ge-Si, Ge-Ge, and Si-Si (unconfined) vibrations. Also shown in Fig.4(a) is the result calculated neglecting the phonon confinement for comparison. It can be seen that the phonon confinement actually enhances the intrasubband scattering process. However, the opposite is true for the intersubband process to be shown below. Fig.4(b) shows the same result as a function of the Ge content in the alloy for the well width of 40Å. The difference increases with the increase of the Ge content since the contributions from the confined phonons will increase while that from the unconfined Si-Si vibration decreases.

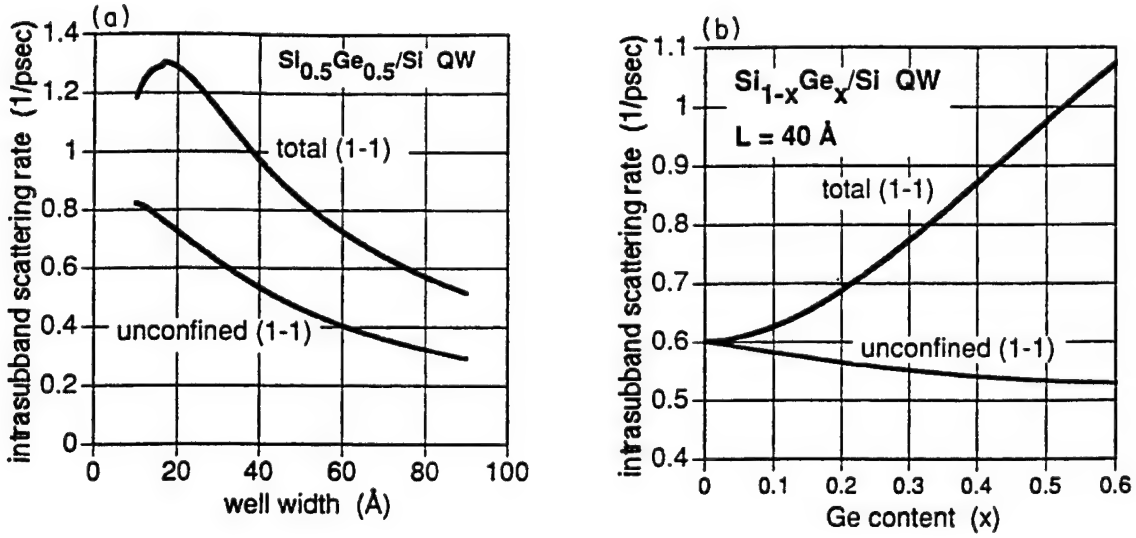

Figure 4. Total intrasubband scattering rates in the lowest subband ($n = 1$) due to Ge-Si, Ge-Ge confined modes and Si-Si unconfined modes, compared to the bulk intrasubband scattering rate assuming no confinement. (a) as a function of well width with Ge content $x = 0.5$; (b) as a function of x for a well width of 40Å.

Intersubband Scattering

The intersubband scattering rate was calculated assuming that the transition originated from the bottom of a subband n with zero kinetic energy to another subband ($n' \neq n$). Both phonon absorption and emission processes are considered in the calculation. Fig.5(a) shows the (2-1) scattering rate with the Si-Si, Ge-Si, and Ge-Ge components as a function of well width for a $Si_{0.5}Ge_{0.5}$/Si QW. Subband 2 appears at the well width of $20\mathring{A}$. The total scattering is obtained by summing the contributions derived from the Ge-Si, Ge-Ge, and Si-Si vibrations including both guided and interface modes. But the interface mode scattering is at least two orders of magnitude weaker than the guided mode for the intersubband process. Similar weakness of the interface mode has been shown in a GaAs/Al_xGa_{1-x}As QW.[7] The result assuming no confinement is also shown in Fig.5(a) for comparison. The sharp increase of the scattering rates in the small well width region ($L < 25\mathring{A}$) is once again due to the increasing confinement in the well region of subband 2 which leads to an increase of the interference G-function. Both scattering intensities from Si-Si and unconfined phonons reduce with further increase of the well width. Since initially the narrow well width only allows a small number of guided modes, the guided mode scattering is weak compared to the Si-Si scattering and the total scattering rate follows the dependence of Si-Si vibration. As the number of allowed guided modes increases with increasing well width, the guided mode scattering actually surpasses the Si-Si component, leading to an increase of the total scattering rate. The small discontinuous incremental steps in the Ge-Si, Ge-Ge, and therefore total scattering curves, are due to the discrete nature of the increase in the number of allowed guided modes as the well width increases. The sudden drops in the curves occur when the energy separation between the two subbands reduces to less than one of the three phonon energies corresponding to different vibrations. Specifically, the drops occurred at $L = 72,\ 83,\ 99\mathring{A}$ correspond to Si-Si phonon ($64.3meV$), Ge-Si phonon ($50.8meV$), and Ge-Ge phonon ($37.4meV$), respectively. It can be seen in Fig.5(a) that the phonon confinement reduces the scattering rate by a factor of two to four as compared to the case of no confinement. It is therefore important to take into account the phonon confinement effect in estimating the subband lifetimes.

Fig.5(b) shows the (2-1) scattering rates as a function of Ge content in the $Si_{1-x}Ge_x$ alloy for a well thickness of $40\mathring{A}$. The contributions from the guided modes increases with the Ge content while the unconfined Si-Si component reduces. As a result, the difference between the total scattering rate and the rate obtained assuming no confinement widens with Ge content.

IV. SUMMARY AND DISCUSSION

In an earlier paper we treated phonon-induced intersubband transitions in $Si_{1-x}Ge_x$/Si MQW structures.[1] The absence of polar optical scattering resulted in subband lifetimes an order of magnitude larger than those in MQWs of III-V semiconductors and without

the precipitous decrease at the optical phonon threshold. This earlier work assumed unconfined, three dimensional phonons. Noting strong experimental evidence for phonon confinement in $Si_{1-x}Ge_x/Si$ MQWs, the present paper extends the earlier treatment to the case in which phonons are confined.

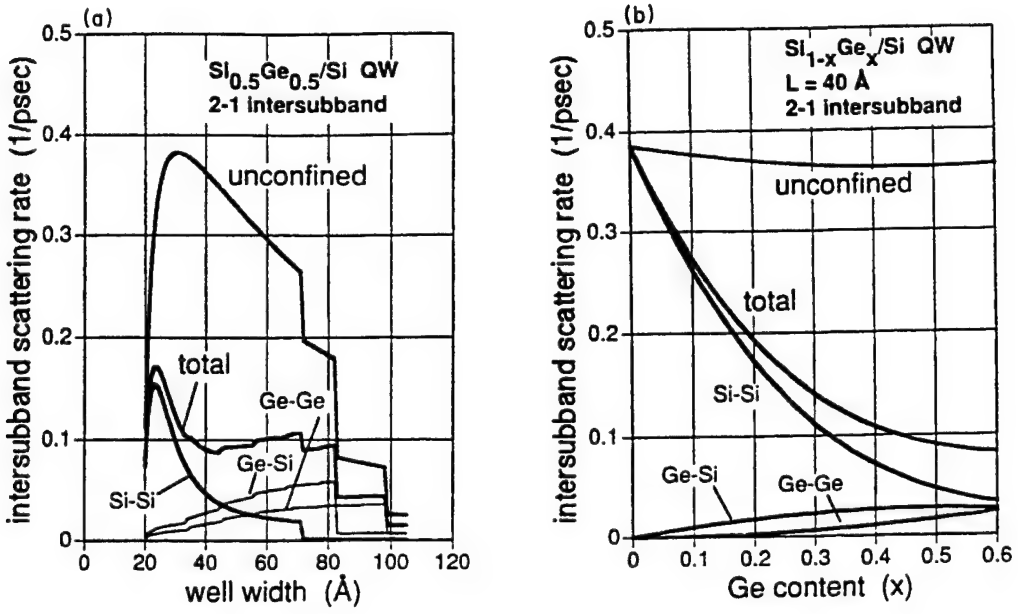

Figure 5. Total intersubband scattering rates from subband 2 to 1 due to Ge-Si, Ge-Ge confined modes and Si-Si unconfined modes, compared to the bulk intersubband scattering rate assuming no confinement. (a) as a function of well width with Ge content $x = 0.5$; (b) as a function of x for a well width of $40\mathring{A}$.

A single $Si_{1-x}Ge_x$ QW with Si barrier is considered. The decoupled heavy-hole subbands and wavefunctions are determined by the finite square well model. Assigning statistical weights to the Si-Si, Ge-Si, and Ge-Ge vibrations in the QW assuming a purely random bond model, the Ge-Si and Ge-Ge modes are treated as confined while the Si-Si modes are extended. The confined modes are of two kinds, guided modes and interface modes. The guided modes consist of the s-TO and coupled LO and p-TO modes, with the boundary condition that the displacements vanish at the interfaces. In comparison with the guided modes for polar optical phonons, the current choice of basis set which describes the coupling between the p-TO and LO modes are neither orthogonal nor complete. Hence, the sum rule found for polar LO phonons cannot be applied to the case of nonpolar optical phonons. The interface mode is obtained applying hydrodynamic boundary conditions to the LO and TO modes separately and then requiring that the z-component of their sum (not the x-component) vanish at the interfaces. The LO mode is a two-dimensional bulk-type solution with constant amplitude in the well and propagating parallel to the interface; the TO mode is an even function (referring to the z-component) with a sinusoidal spatial dependence so that the boundary conditions at

the interfaces can be satisfied.

The Ge-Ge optical phonon spectrum in the well region has no overlap with that of Si-Si optical phonons in the barriers, but instead overlaps with that of the acoustic Si phonons. The model for the interface mode derived from the optical phonon dispersion relations using the hydrodynamic boundary conditions is not without criticism. Further investigation of this subject is underway to provide a more accurate estimate of the intrasubband scattering rates. But we would still expect the intersubband process to be dominated by the guided-mode scattering, which ultimately determines the subband lifetimes.

The intrasubband and intersubband scattering rates are calculated as a function of the QW structure parameters: Ge content, x, in the $Si_{1-x}Ge_x$ well and the well width, L. These parameters are varied within the limits reportedly to produce the metastable strained layers of $Si_{1-x}Ge_x$ alloy on Si substrates without introducing a large number of misfit defects. We choose the Ge content of $x = 0.5$ as we vary the well width to give a fair weight of the Ge-Si and Ge-Ge confined modes. We use the fixed well width of $40\mathring{A}$ to allow at least two confined heavy-hole subbands as we vary the Ge content. Our results are as follows. For intrasubband scattering, the scattering by the interface mode is nearly the same as that for the guided mode (Fig.3), and the total intrasubband scattering with confinement is larger than that without confinement (Fig.4). However for intersubband scattering, the interface mode scattering is at least two orders of magnitude smaller than that for the guided mode. Finally, as can be seen from Fig.5, the total intersubband scattering rate with confinement is a factor of two to four smaller than that which would be obtained assuming no confinement. Thus, one would expect a factor of two to four enhancement in the intersubband lifetimes which determine population inversion in an intersubband laser.

Finally, we note that the present investigation has considered the scattering of heavy holes whose dispersion is parabolic. The extension to light holes and the split-off band, which are coupled due to spin-orbit coupling and strain[25] and whose dispersions are therefore nonparabolic, would require expension of the theory, but with similar results anticipated.

Part II. A study of confined optical phonons in Si/ZnS superlattices

I. INTRODUCTION

There is an interest in moving the lasing from the far- and mid-infrared range to the near-infrared optical communications wavelengths, $\lambda = 1.3$ or $1.55\mu m$[29]. Since the latter wavelength corresponds to a photon energy of $800meV$, the $Si_{1-x}Ge_x$/Si heterosystem is inadequate because a maximum practical valence band offset of only $\sim 500meV$ can be obtained for pseudomorphic $Si_{1-x}Ge_x$ layers at $x = 0.5 \sim 0.6$. Therefore, alternative large- bandgap, nearly lattice-matched barrier materials for Si quantum wells must be sought; materials with sufficiently large band offsets with respect to silicon. Possible candidates include, ZnS, BeSeTe, CaF_2, SiO_x, SiO_2, the Si/SiO_2 superlattice, and γ-Al_2O_3, among others[29]-[31]. The Si/ZnS heterosystem has received the most attention as current advances in epitaxy technology have allowed the growth of heterostructures consisting of polar and nonpolar materials[32, 33]. The lattice mismatch of cubic ZnS with respect to Si is only 0.3%. The valence band offset has been predicted theoretically[34]-[37], while recent experiments[38] show that the value is close to $1.5eV$, sufficiently large to give intersubband energy differences in the desired $800meV$ range. MBE growth of ZnS upon Si, and Si upon ZnS have been demonstrated[33], with the use of an As monolayer to satisfy the local bonding requirements, although the effect of the monolayer on the offsets has not been determined.

The possibility of population inversion and the operation of intersubband lasers depend critically on the lifetimes of the involved subbands. The subband lifetimes in turn are determined by nonradiative phonon scattering processes. The purpose of the present paper is to study the optical phonon modes and their interaction with carriers in the Si/ZnS system since the optical phonon scattering is considered to be dominant in the phonon scattering processes. This combination of materials is new, since it consists of both a nonpolar and polar semiconductor. Previous studies in carrier scattering by confined optical phonons in heterostructures have been focused only on one type of phonons, either polar[7]-[10] or nonpolar[3]-[4]. In the current situation involving both polar and nonpolar materials, carrier scattering by both types of phonons needs to be considered. To the best of our knowledge, there has not been any reported investigation on this mixed nature of optical phonons, their confinement effect, and their interaction with carriers in a heterostructure. In this paper, we will present a theoretical study based on the macroscopic continuum model to describe the confined optical phonon modes and will use this model to calculate the optical-phonon scattering of heavy holes in a heterostructure consisting of polar (ZnS) and nonpolar materials (Si), as we are interested in the feasibility of constructing an intersubband laser within the valence band of the Si/ZnS heterostructure. This valence intersubband laser will likely be a quantum-parallel superlattice laser[40] or a quantum cascade laser. Our latest thinking[41] is that each of the N laser periods will consists of one square Si quantum well containing two active heavy-hole subbands. Due to the non-parabolicity of these subbands, we believe that a population inversion, localized in k-space, can be engineered between

the subbands. In this investigation, we will consider a simple superlattice comprised of alternating layers of Si and ZnS, much like the flat-band superlattice of the quantum parallel laser (Fig.2(b) of [40]). The results of this study will provide the basis for the calculation of subband lifetimes required to determine laser gain and threshold.

As described below in greater detail, since the optical dispersions (frequency versus wavevector) of the silicon ($\hbar\omega_{Si} = 64meV$) and zinc sulphide ($\hbar\omega_{ZnS} = 43meV$) have no overlap, the optical phonons are assumed to be totally confined in both materials. In the silicon layers, a continuum model with double hybridization of the longitudinal optical (LO) and transverse optical (TO) modes is used to describe the vibration patterns of the guided modes as described in Part I. The only boundary condition that needs to be satisfied in the Si layers is the vanishing of the displacements at the Si-ZnS interface, since the ZnS layers can be considered as infinitely rigid with respect to the vibrations of the Si layer. Hence, there is no interface mode in the Si layers. The situation on the ZnS layers is more complex. Following the work by Ridley[8, 9], here a continuum model is employed with hybridization of the optical LO, TO, and interface polariton (IP) modes needed to satisfy both the mechanical and electrostatic boundary conditions at the interfaces. Specifically, the electrostatic boundary conditions are the continuity of E_x, the electric field parallel to the interface, and the continuity of D_z, the displacement field normal to the interface. The mechanical boundary condition is again the vanishing of the optical displacements since the Si layers can be considered as infinitely rigid with respect to the vibrations of the ZnS layers.

Our current work provides a complete set of analytical expressions for the optical phonon dispersion relations, optical displacements, and associated scalar and vector potentials. These expressions are subsequently used in calculating the interaction of heavy holes with the confined optical phonons. In Section II, we establish a continuum model for the optical displacement modes in Si and ZnS layers satisfying both mechanical and electrical boundary conditions. In section III, we outline a numerical procedure for determining the frequency of a ZnS optical mode inducing the intersubband scattering. In Section IV, we describe the scalar and vector potentials associated with the ZnS ionic displacement modes. In Section V, we summarize and discuss our results and conclusions.

II. Mode Patterns

A continuum model for the optical modes in the Si/ZnS superlattice is employed. Both mechanical and electrical boundary conditions are satisfied at the heterointerfaces. Since the optical dispersion relations (frequency versus phonon wavevector) in the two bulk materials have no overlap, the phonons are taken to be confined in their respective materials. For the Si layers, the continuum model for optical phonons in nonpolar materials is used. Here double hybridization of the LO (longitudinal optical) and TO (transverse optical) modes is used to give the vibration patterns of the guided modes. Since the ZnS layers are infinitely rigid with respect to the vibrations of the Si layers, only

the mechanical boundary condition, the vanishing of the displacements at the interfaces, has to be satisfied.

For the polar ZnS layers, the situation is more complex and an alternate continuum model[8, 9] consisting of an intermixing of confined LO, TO, and IP (interface polariton) modes is needed in order to satisfy both the electrostatic and mechanical boundary conditions. The boundary conditions which must be satisfied are (1) the continuity of E_x, the component of electric field parallel to the interface, (2) the continuity of D_z, the component of the displacement vector normal to the interface, and (3) the vanishing of the vector displacement u at the interface.

A. Modes in Si Layers

As discussed in detail in Part I, using the boundary condition that $\mathbf{u} = 0$ at the interfaces gives for the s-TO mode

$$u_y = Ae^{iq_x x}\sin(q_z z), \qquad \text{with } q_z = \frac{n\pi}{d_{Si}} \tag{29}$$

where $n = 1, 2, \cdots$ and A is a mode coefficient. This mode does not mix with other modes.

The hybrid LO and p-TO modes admit two classes of solutions. The 'sine' solution is

$$\begin{aligned} u_x &= 2Be^{iq_x x}q_x[\cos(q_L z) - \cos(q_T z)], \\ u_z &= 2iBe^{ik_x x}[q_L \sin(q_L z) + \frac{q_x^2}{q_T}\sin(q_T z)], \end{aligned} \tag{30}$$

and the 'cosine' solution is

$$\begin{aligned} u_x &= 2iBe^{iq_x x}[q_x \sin(q_L z) + \frac{q_L q_T}{q_x}\sin(q_T z)], \\ u_z &= 2Be^{iq_x x}q_L[\cos(q_L z) - \cos(q_T z)] \end{aligned} \tag{31}$$

where

$$q_L = \frac{n_L\pi}{d_{Si}} \quad \text{and} \quad q_T = \frac{n_T\pi}{d_{Si}}, \tag{32}$$

where $n_L = 1, 2, \cdots$, $n_T = 3, 4, \cdots$, $n_T - n_L = 2, 4, 6, \cdots$, and B is a mode coefficient. No interface modes exist in the Si layer because of the boundary condition $\mathbf{u} = 0$.

The lowest s-TO mode pattern in Eq.(29) for $q_z = \pi/d_{Si}$ is shown in Fig.6(a) within a Si layer of $d_{Si} = 40\text{Å}$, while the hybrid patterns of the lowest p-TO and LO modes with $q_L = \pi/d_{Si}$ and $q_T = 3\pi/d_{Si}$ are shown in Figs.6(b) and 6(c) for the 'sine' and 'cosine' solutions given in Eqs.(30) and (31), respectively within the same Si layer. The strict confinement which requires the vanishing of ionic displacements at the boundaries

of Si layers is clearly demonstrated for both vibration modes.

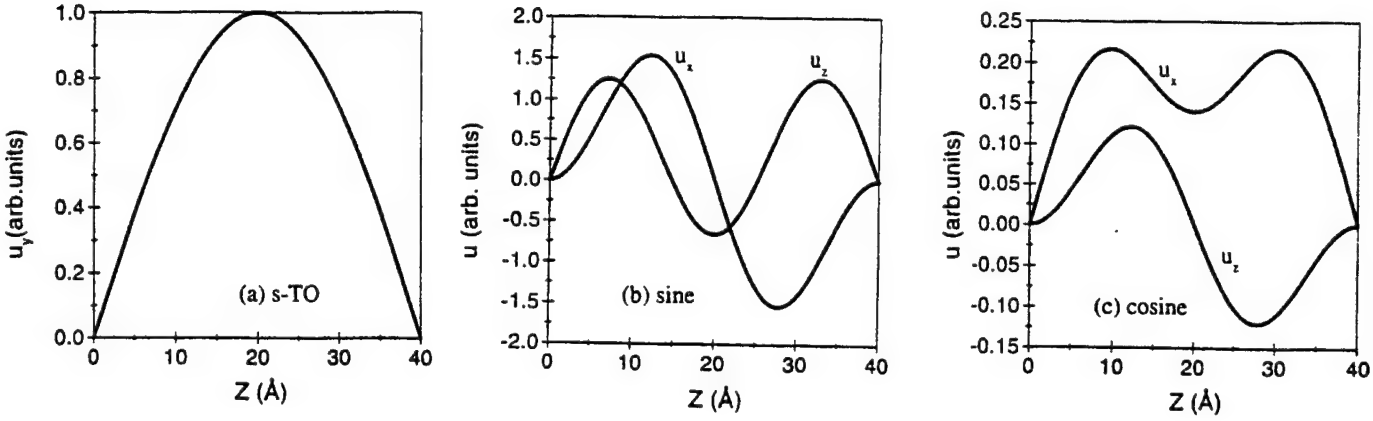

Figure 6. Vibration patterns in a Si layer with a width of 40Å for (a) the guided s-TO mode, (b) the 'sine' solution, and (c) the 'cosine' solution of the guided p-TO and LO modes.

B. Modes in ZnS Layers

The boundary conditions are the continuity of E_x, D_z, and the vanishing of $\mathbf{u}$ at the interfaces. These conditions can be satisfied by a unique linear combination of LO, TO, and IP modes with common frequency and common in-plane wavevector q_x,

$$\mathbf{u} = \mathbf{u}_{LO} + \mathbf{u}_{TO} + \mathbf{u}_{IP}. \tag{33}$$

We will use this hybrid expression to calculate the electrical interaction with carriers which is considerably stronger than the optical deformation potential interaction. We need consider only the displacements u_x and u_z, since u_y associated with the s-TO mode has no related electric field and therefore does not interact with carriers electrically. Once again, the expressions are obtained by taking the Bloch superlattice wavevector $q_{SL} = 0$.

For the LO mode, the ionic displacements are

$$\begin{aligned} u_x &= e^{i(q_x x - \omega t)} q_x (A_L e^{iq_L z} + B_L e^{-iq_L z}), \\ u_z &= e^{i(q_x x - \omega t)} q_L (A_L e^{iq_L z} - B_L e^{-iq_L z}). \end{aligned} \tag{34}$$

which is confined within the ZnS layer with a width of d_{ZnS}, $-d_{ZnS}/2 < z < d_{ZnS}/2$

The associated electric fields are

$$E_x = -\rho_o u_x, \qquad E_z = -\rho_o u_z, \tag{35}$$

where

$$\rho_o = \frac{e^*}{\epsilon_o \Omega}, \tag{36}$$

with the effective ionic charge

$$e^{*2} = M\Omega\omega_{LO}^2\epsilon_o^2(\frac{1}{\epsilon_\infty} - \frac{1}{\epsilon_s}), \tag{37}$$

where M is the reduced mass, ϵ_o is the permittivity of free space, ϵ_∞, ϵ_s are the high-frequency and static permittivities, and Ω is the volume of primitive unit cell. The scalar potential ϕ associated with the electric field $\mathbf{E} = -\nabla\phi$ is in turn given as

$$\phi = -i\rho_o e^{i(q_x x - \omega t)}(A_L e^{iq_L z} + B_L e^{-iq_L z}). \tag{38}$$

For the TO mode

$$\begin{aligned} u_x &= e^{i(q_x x - \omega t)} q_T (A_T e^{iq_T z} + B_T e^{-iq_T z}), \\ u_z &= -e^{i(q_x x - \omega t)} q_x (A_T e^{iq_T z} - B_T e^{-iq_T z}). \end{aligned} \tag{39}$$

The electric fields associated with this mode are negligible.

For the IP mode

$$\begin{aligned} u_x &= e^{i(q_x x - \omega t)} q_p (A_P e^{iq_p z} + B_P e^{-iq_p z}), \\ u_z &= ie^{i(q_x x - \omega t)} q_p (A_P e^{iq_p z} - B_P e^{-iq_p z}) \end{aligned} \tag{40}$$

The associated electric fields are

$$E_x = -\rho_p u_x, \qquad E_z = -\rho_p u_z, \tag{41}$$

where

$$\rho_p = \rho_o \frac{\omega^2 - \omega_{TO}^2}{\omega_{LO}^2 - \omega_{TO}^2}, \tag{42}$$

and ω_{LO} and ω_{TO} are bulk ZnS LO and TO optical phonon frequencies at Γ point, respectively. The electric fields associated with the interface modes propagate into the Si layers although they are treated as infinitely rigid and do not contain ZnS ionic displacement.

Being a transverse electromagnetic wave, there is a vector potential $\mathbf{A}$ associated with the electric field $\mathbf{E} = -\partial\mathbf{A}/\partial t$. Within the ZnS layers,

$$\begin{aligned} A_x &= i\frac{\rho_p}{\omega} e^{i(q_x x - \omega t)} q_p (A_P e^{iq_p z} + B_P e^{-iq_p z}), \\ A_z &= -\frac{\rho_p}{\omega} e^{i(q_x x - \omega t)} q_p (A_P e^{iq_p z} - B_P e^{-iq_p z}) \end{aligned} \tag{43}$$

While in the Si layers, a similar expression can be obtained with another set of mode coefficients, A_{p1} and B_{p1}.

Since large in-plane wavevectors are likely to be involved when dealing with carrier transitions due to optical phonons between two subbands separated with a relatively large energy, we have endeavored to obtain analytical dispersions of the LO and TO

optical branches by curve-fitting the experimental bulk phonon dispersions for the entire Brillioun zone. The requirement for common frequency yields,

$$\begin{aligned} \omega &= \omega_{LO} - \beta_L(q_x^2 + q_L^2) \\ &= \omega_{TO} - \beta_T(q_x^2 + q_T^2) \\ &= \frac{c(q_x^2 + q_p^2)^{1/2}}{n(\omega)} \end{aligned} \tag{44}$$

where $\beta_L = 0.808 THz \cdot \AA^2$ and $\beta_T = 2.194 THz \cdot \AA^2$ are obtained from curve-fitting the bulk ZnS optical phonon dispersions, c is the velocity of light in vacuum, and $n(\omega)$ is the index of refraction. In the above expressions, the frequency in the ZnS layers lies between the ZnS LO and TO zone center frequencies. Since $\omega_{TO} < \omega_{LO}$, in order for the TO frequency to be equal to a LO frequency q_T must be imaginary $q_T = iq_o$, corresponding to a TO interface mode. The modes which interact most strongly with carriers are those with frequencies near the LO branch. For these modes, the value of q_o is large, and we can take the approximation

$$\tanh(q_o d_{ZnS}) \approx 1. \tag{45}$$

In the unretarded limit ($c \to \infty$), $q_x^2 + q_p^2 \approx 0$ for the IP mode. Hence, $q_p \approx iq_x$.

Applying, at the two interfaces between layers Si and ZnS in a period of the superlattice, the conditions that u_x and u_z equal to zero along with the continuity of E_x and D_z, leads to eight simultaneous equations involving the eight unknown mode coefficients ($A_L, B_L; A_T, B_T; A_P, B_P$; and A_{P1}, B_{P1}). The following two ionic displacement mode patterns emerge for the hybrid in Eq.(33) taking the Bloch superlattice wavevector $q_{SL} = 0$ and the approximation $\tanh(q_o d_{ZnS}) \approx 1$. Both ionic displacement patterns are confined within the ZnS layer, $-d_{ZnS}/2 < z < d_{ZnS}/2$. For the first type,

$$\begin{aligned} u_x = \; & 2iBe^{iq_x x} q_x \{\sin(q_L z) \\ & -[1 - p_1 \tanh(q_x d_{ZnS}/2)] \sin(q_L d_{ZnS}/2) \frac{\sinh(q_o z)}{\sinh(q_o d_{ZnS}/2)} \\ & -p_1 \sin(q_L d_{ZnS}/2) \frac{\sinh(q_x z)}{\cosh(q_x d_{ZnS}/2)}\}, \\ u_z = \; & 2Be^{iq_x x} q_L \{\cos(q_L z) \\ & -\frac{q_x^2}{q_L q_o}[1 - p_1 \tanh(q_x d_{ZnS}/2)] \sin(q_L d_{ZnS}/2) \frac{\cosh(q_o z)}{\sinh(q_o d_{ZnS}/2)} \\ & -\frac{q_x}{q_L} p_1 \sin(q_L d_{ZnS}/2) \frac{\cosh(q_x z)}{\cosh(q_x d_{ZnS}/2)}\}, \end{aligned} \tag{46}$$

and for the second type,

$$
\begin{aligned}
u_x = \; & 2Be^{iq_x x} q_x \{\cos(q_L z) \\
& -[1 - p_2 \coth(q_x d_{ZnS}/2)] \cos(q_L d_{ZnS}/2) \frac{\cosh(q_o z)}{\sinh(q_o d_{ZnS}/2)} \\
& -p_2 \cos(q_L d_{ZnS}/2) \frac{\cosh(q_x z)}{\sinh(q_x d_{ZnS}/2)}\}, \\
u_z = \; & 2iBe^{iq_x x} q_L \{\sin(q_L z) \\
& +\frac{q_x^2}{q_L q_o}[1 - p_2 \coth(q_x d_{ZnS}/2)] \cos(q_L d_{ZnS}/2) \frac{\sinh(q_o z)}{\sinh(q_o d_{ZnS}/2)} \\
& +\frac{q_x}{q_L} p_2 \cos(q_L d_{ZnS}/2) \frac{\sinh(q_x z)}{\sinh(q_x d_{ZnS}/2)}\},
\end{aligned}
\tag{47}
$$

where

$$
\begin{aligned}
p_1 &= \frac{\cosh(q_x d_{Si}/2) \cosh(q_x d_{ZnS}/2)}{d}, \\
p_2 &= \frac{\sinh(q_x d_{Si}/2) \sinh(q_x d_{ZnS}/2)}{d}, \\
d &= r \sinh(q_x d_{Si}/2) \cosh(q_x d_{ZnS}/2) + \sinh(q_x d_{ZnS}/2) \cosh(q_x d_{Si}/2), \\
r &= \frac{\epsilon_{p1}}{\epsilon_{p2}},
\end{aligned}
\tag{48}
$$

and ϵ_{p1} and ϵ_{p2} are the permittivities in Si and ZnS layers, respectively, with

$$
\epsilon_{p2} = \epsilon_\infty \frac{\omega^2 - \omega_{LO}^2}{\omega^2 - \omega_{TO}^2}. \tag{49}
$$

To illustrate the patterns of ionic displacements in the ZnS layers given in Eqs.(46) and (47), we need to first determine values for q_x, q_L, and q_o. To do so, we will follow the numerical procedure described in Section III by arbitrarily fixing a value for the in-plane phonon wavevector $q_x = \pi/(5a_{ZnS})$, where a_{ZnS} is the lattice constant of ZnS. In calculating the carrier-optical phonon interaction, the value of q_x is actually determined by the conservation of in-plane momentum between the initial and final states of the scattering process. For a given value of q_x, typically, a set of hybridized modes can be obtained. Here, we show only the mode pattern with frequency close to ω_{LO}.

We obtained $\hbar\omega = 41meV$, $q_L = 0.46 \times 10^8/cm$ and $q_o = 0.48 \times 10^8/cm$. Substituting these values into Eqs.(46) and (47), we obtained Figs.7(a) and 7(b) showing the mode patterns of ionic displacement of both the first and second types, respectively in a ZnS layer of $d_{ZnS} = 20\text{Å}$. It can be seen from Figs.7(a) and 7(b) that the mechanical boundary condition, vanishing of the ionic displacements at the interfaces of Si and ZnS

layers, is satisfied.

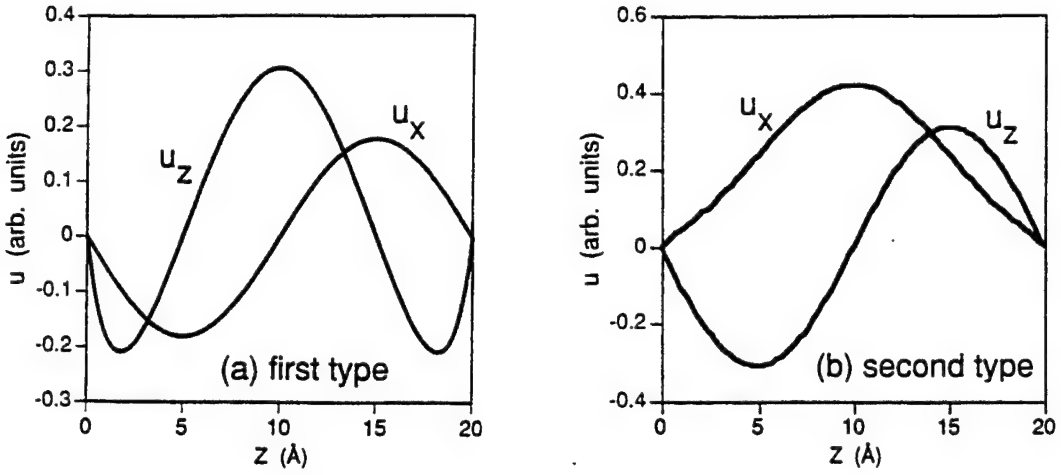

Figure 7. Vibration patterns in a ZnS layer with a width of 20Å for (a) the first type and (b) the second type solutions of the hybridized LO, TO and IP modes.

III. Dispersion Relationship

The phonon frequency in the ZnS layers is determined by the following set of equations;

$$\begin{cases} \omega = \omega_{LO} - \beta_L(q_x^2 + q_L^2), \\ \omega = \omega_{TO} - \beta_T(q_x^2 - q_o^2), \\ t_1 + t_2\cos(q_L d_{ZnS}) + t_3\sin(q_L d_{ZnS}) = 0 \end{cases} \tag{50}$$

where

$$\begin{aligned} t_1 = \;& 4p\sinh(q_x d_{Si}) + 4pr\sinh(q_x d_{ZnS}), \\ t_2 = \;& -4p\alpha, \\ t_3 = \;& 8p^2 r\sinh(q_x d_{ZnS})\sinh(q_x d_{Si}) - 4p^2\alpha^2 \\ & +4p^2 r^2\sinh^2(q_x d_{ZnS}) + 4p^2\sinh^2(q_x d_{Si}) + 1, \end{aligned} \tag{51}$$

with

$$p = \frac{q_x}{4q_L r s d} \tag{52}$$

and

$$s = \frac{\omega^2 - \omega_{TO}^2}{\omega_{LO}^2 - \omega_{TO}^2}. \tag{53}$$

The third equation in (50) is obtained from the requirement of a nonzero solution for the eight simultaneous equations discussed above, and Eq.(51) is arrived at under the approximation, $\tanh(q_o d_{ZnS}) \approx 1$.

The numerical procedure for determining a phonon frequency is the following: given a value of q_x, we can determine those of t_1, t_2, and t_3 from Eq.(51). Then ω is scanned from ω_{TO} to ω_{LO}. For a given value of ω, q_L and q_o are obtained from the first

two equations in (50). Those values are then substituted into the third equation in (50) to determine if the particular value of ω is a solution.

IV. Scalar and Vector Potentials

Associated with the two types of ionic displacement in Eqs.(46) and (47), the scalar potentials in ZnS layers are given as, for the first type,

$$\phi = \begin{cases} 2\rho_o B e^{iq_x x}\sin(q_L z_1) & |z_1| < \dfrac{d_{ZnS}}{2} \quad \text{ZnS layer,} \\ 0 & |z_2| < \dfrac{d_{Si}}{2} \quad \text{Si layer,} \end{cases} \tag{54}$$

and for the second type,

$$\phi = \begin{cases} -2i\rho_o B e^{iq_x x}\cos(q_L z_1) & |z_1| < \dfrac{d_{ZnS}}{2} \quad \text{ZnS layer,} \\ 0 & |z_2| < \dfrac{d_{Si}}{2} \quad \text{Si layer.} \end{cases} \tag{55}$$

Note that we have used two different coordinates z_1 and z_2 for layers ZnS and Si, respectively, with their origins placed at the centers of the respective layers.

The vector potentials can be obtained, for the first type,

$$A_x = \begin{cases} \dfrac{2s\rho_o q_x}{\omega} B e^{iq_x x} p_1 \sin(q_L d_{ZnS}/2)\dfrac{\sinh(q_x z_1)}{\cosh(q_x d_{ZnS}/2)} & |z_1| < \dfrac{d_{ZnS}}{2} \quad \text{ZnS layer,} \\ \dfrac{4q_x\rho_o}{\omega} B e^{iq_x x} V_1 \sinh(q_x z_2) & |z_2| < \dfrac{d_{Si}}{2} \quad \text{Si layer,} \end{cases} \tag{56}$$

$$A_z = \begin{cases} \dfrac{2is\rho_o q_x}{\omega} B e^{iq_x x} p_1 \sin(q_L d_{ZnS}/2)\dfrac{\cosh(q_x z_1)}{\cosh(q_x d_{ZnS}/2)} & |z_1| < \dfrac{d_{ZnS}}{2} \quad \text{ZnS layer,} \\ \dfrac{4iq_x\rho_o}{\omega} B e^{iq_x x} V_1 \cosh(q_x z_2) & |z_2| < \dfrac{d_{Si}}{2} \quad \text{Si layer,} \end{cases} \tag{57}$$

and for the second type,

$$A_x = \begin{cases} -\dfrac{2is\rho_o q_x}{\omega} B e^{iq_x x} p_2 \cos(q_L d_{ZnS}/2)\dfrac{\cosh(q_x z_1)}{\sinh(q_x d_{ZnS}/2)} & |z_1| < \dfrac{d_{ZnS}}{2} \quad \text{ZnS layer,} \\ \dfrac{4iq_x\rho_o}{\omega} B e^{iq_x x} V_2 \cosh(q_x z_2) & |z_2| < \dfrac{d_{Si}}{2} \quad \text{Si layer,} \end{cases} \tag{58}$$

$$A_z = \begin{cases} -\dfrac{2s\rho_o q_x}{\omega} B e^{iq_x x} p_2 \cos(q_L d_{ZnS}/2)\dfrac{\sinh(q_x z_1)}{\sinh(q_x d_{ZnS}/2)} & |z_1| < \dfrac{d_{ZnS}}{2} \quad \text{ZnS layer,} \\ \dfrac{4q_x\rho_o}{\omega} B e^{iq_x x} V_2 \sinh(q_x z_2) & |z_2| < \dfrac{d_{Si}}{2} \quad \text{Si layer,} \end{cases} \tag{59}$$

where

$$V_1 = \frac{r\sin(q_L d_{ZnS}/2)\cosh(q_x d_{ZnS}/2)}{2d},$$
$$V_2 = \frac{r\cos(q_L d_{ZnS}/2)\sinh(q_x d_{ZnS}/2)}{2d}, \tag{60}$$

and p_1, p_2, and d are given in Eq.(48).

The scalar potentials associated with the LO modes are strictly confined within the ZnS layers. Their distributions are shown in Fig.8 for the first and second types given in Eqs.(54) and (55) with $q_L = 0.31 \times 10^8/cm$, $d_{ZnS} = 20\mathring{A}$, respectively.

The vector potential associated with the IP modes are distributed in both Si and ZnS layers, even though Si layers are treated as infinitely rigid and do not contain ZnS ionic displacements. The profiles for the two components of the vector potentials given in Eqs.(56-59) for the first and second types with $d_{Si} = 40\mathring{A}$, $d_{ZnS} = 20\mathring{A}$ are shown in Figs.9(a) and 9(b), respectively.

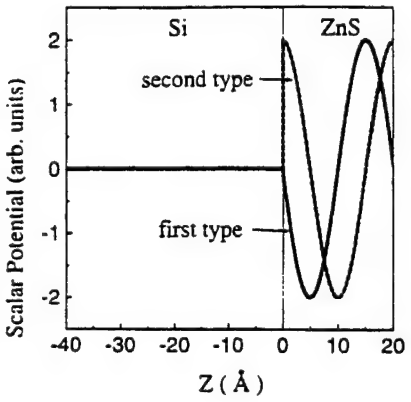

Figure 8. Scalar potential distribution associated with the LO modes in a period of the Si/ZnS superlattice with $d_{Si} = 40\mathring{A}$ and $d_{ZnS} = 20\mathring{A}$ for both the first and second types of the vibration modes.

It can be seen from Figs.8 and 9 that both scalar and vector potentials are not continuous across the interfaces. However, as pointed by Ridley[9], the energy of interaction with an electron traveling coherently with the optical phonon is continuous. The electric field can be obtained as

$$\mathbf{E} = -\nabla\phi - \frac{\partial \mathbf{A}}{\partial t}. \tag{61}$$

The continuity of E_x and $D_z = \epsilon(\omega)E_z$ implies that at the boundaries,

$$\omega A_x|_{z_2=\pm d_{Si}/2} = -q_x\phi|_{z_1=\mp d_{ZnS}/2} + \omega A_x|_{z_1=\mp d_{ZnS}/2},$$
$$A_z|_{z_2=\pm d_{Si}/2} = r A_z|_{z_1=\mp d_{ZnS}/2}, \tag{62}$$

where A_{1x} and A_{1z} are x- and z-components of the vector potential in Si layers. The interaction in the Si layer is $e(A_{1x}v_x + A_{1z}v_z)$ and in the ZnS layer $e(-\phi + A_x v_x + A_z v_z)$, which are equal when the electron velocity $v_x = \omega/q_x$ and $v_z = 0$. Thus, the coherent interaction energy is continuous across the interfaces.

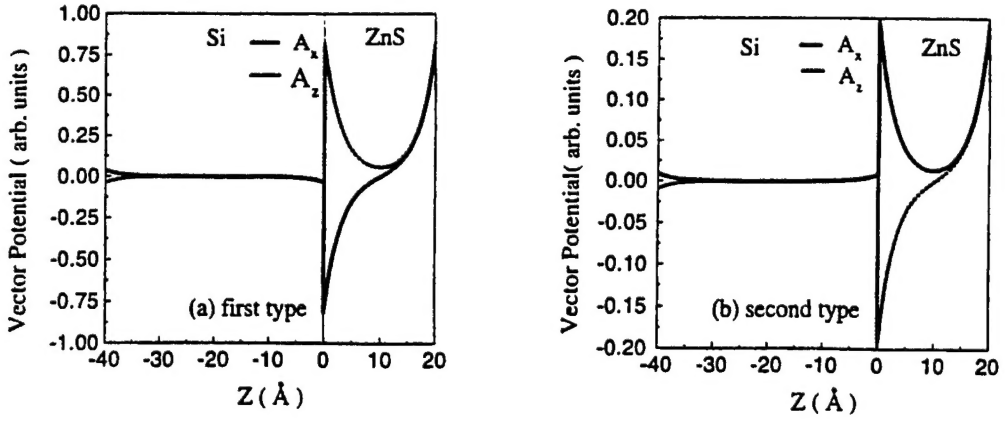

Figure 9. Vector potentials associated with the IP modes distributed in a period of the Si/ZnS superlattice with $d_{Si} = 40\mathring{A}$ and $d_{ZnS} = 20\mathring{A}$ for (a) the first type and (b) the second type of the vibration modes.

The electric field distributions for E_x and $\epsilon(\omega)$ in Si ($d_{Si} = 40\mathring{A}$) and ZnS ($d_{ZnS} = 40\mathring{A}$) layers are shown in Figs.10(a) and 10(b) for the first and second types, respectively. The continuity of E_x and D_z across the Si and ZnS interface according to Eq.(62) is clearly demonstrated.

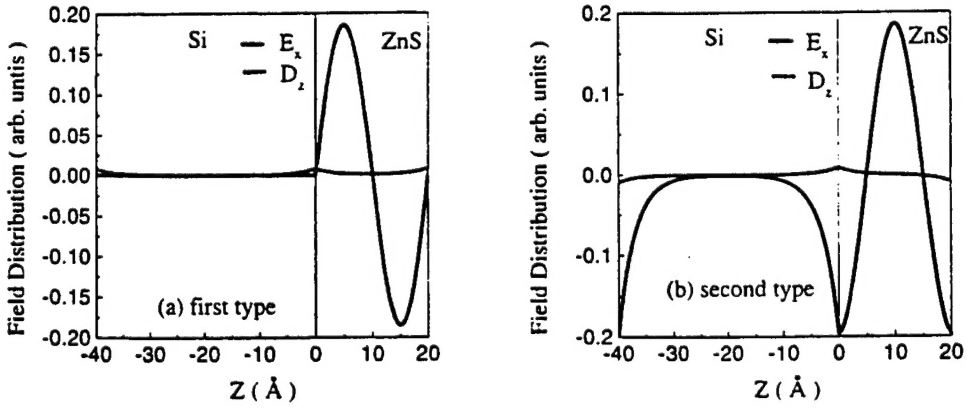

Figure 10. The field distributions, E_x and D_z, derived from the scalar and vector potentials, in a period of the Si/ZnS superlattice with $d_{Si} = 40\mathring{A}$ and $d_{ZnS} = 20\mathring{A}$ for (a) the first type and (b) the second type of the vibration modes.

V. Summary and Discussion

We have provided an analytical model of optical modes in Si/ZnS superlattices consisting of polar and nonpolar optical phonons. This is a new procedure for obtaining the eigen modes of a mixed polar-nonpolar heterosystem. In the Si layers, a continuum model with double hybridization of the LO and TO modes is used to describe the vibration patterns. Since there is no electric field resulting from the nonpolar ionic displacements in Si layers, the only boundary condition that needs to be satisfied in the Si layers is the vanishing of the displacements at the Si-ZnS interface, as the ZnS layers can be considered as infinitely rigid with respect to the vibrations of the Si layer. Due to this strict confinement, only guided modes emerge in the Si layers which consist of s-TO and coupled p-TO and LO modes, with no interface modes. These guided modes have been illustrated. Their interaction with carriers in the superlattice can be calculated through the optical deformation potential for Si. The interaction Hamiltonian can be obtained by taking the product of this potential with the normalized ionic displacement.

However, for the optical phonons in ZnS layers, we need to include the electrical interaction in calculating the carrier scattering by optical phonons, since there are electric fields associated with the polar optical vibrations. As a result, both mechanical and electrostatic boundary conditions need to be satisfied in the interfaces. A continuum model employing a linear combination of LO, TO and IP (interface polariton) modes with a common frequency is used to describe the ionic displacements in ZnS layers. A numerical procedure for determining a phonon frequency is provided. This hybridized model is necessary to meet the simultaneous requirement on the mechanical and electrostatic boundary conditions. The mechanical boundary condition is again the vanishing of the optical displacements since Si layers can be considered as infinitely rigid with respect to the vibrations of the ZnS layers. The electrostatic boundary conditions are the continuity of the electric field parallel to the interface, and the continuity of the displacement field normal to the interface. Based on this set of boundary conditions, expressions are obtained for the ionic displacements in ZnS layers consisting of LO, TO, and IP modes. There are scalar and vector potentials associated with the LO and IP modes, respectively, but no electric field associated with the TO mode. The scalar potential and its associated electric field due to the LO mode are distributed only within the ZnS layers and are zero in the Si layers. But the vector potential and its associated electric field due to the IP mode have distributions in both ZnS and Si layers even though there is no ZnS ionic displacement mode in the Si layers. Examples of these mode characteristics have been demonstrated. Neither the scalar nor vector potential is continuous across the Si-ZnS interface, but the energy of coherent interaction with carriers is continuous due to the continuity of the electric field parallel to the interface.

References

[1] G. Sun, L. Friedman, and R.A. Soref, Appl. Phys. Lett. **66**, 3425 (1995)

[2] A. Fasolino, E. Molinari, and J.C. Mann, Phys. Rev. B **39**, 3923 (1989)

[3] S. C. Jain and W. Hayes, Semicond. Sci. Technol. **6**, 547 (1991)

[4] B. K. Ridley, Phys. Rev. B **44**, 9002 (1991)

[5] M. Babiker, J. Phys. C: Solid State Phys. **19**, 683 (1986)

[6] M. Babiker, A. Ghosal, and B. K. Ridley, Superlattices and Microstructures **5**, 133 (1989)

[7] B. K. Ridley, Phys. Rev. B **39**, 5282 (1989)

[8] M. P. Chamberlain, M Cardona, and B. K. Ridley, Phys. Rev. B **48**, 14356 (1993)

[9] B. K. Ridley, Phys. Rev. B **47**, 4592 (1993)

[10] N. C. Constantinou and B. K. Ridley, Phys. Rev. B **49**, 17065 (1994)

[11] B. K. Ridley, Appl. Phys. Lett. **66**, 3633 (1995)

[12] F. A. Riddoch and B. K. Ridley, Physica **134B**, 342 (1985)

[13] N. Mori and T. Ando, Phys. Rev. B **40**, 6175 (1989)

[14] K. J. Nash, Phys. Rev. B **46**, 7723 (1992)

[15] L. Register, Phys. Rev. B **45**, 8756 (1992)

[16] H. Akera and T. Ando, Phys. Rev. B **40**, 2914 (1989)

[17] A. Fasolino, E. Molinari, and A. Qteish, Condensed Systems of Low Dimensionality, Edited by J. L. Beeby et al., Plenum Press, New York, 495 (1991)

[18] H. Rucker, E. Molinari, and P. Lugli, Phys. Rev B **45**, 6747 (1992)

[19] E. Molinari and A. Fasolino, Appl. Phys. Lett. **54**, 1220 (1989)

[20] E. Molinari, A. Fasolino, and K. Kunc, Superlattices and Microstructures **2**, 397 (1986)

[21] D. Levi, Shu-Lin Zhang, M. V. Klein, J. Klem, and H. Morkoc, Phys. Rev. B **36**, 8032 (1987)

[22] J. Faist, F. Capasso, D. L. Sivco, A. L. Hutchinson, C. Sirtory, and A. Y. Cho, Science **264**, 553 (1994)

[23] B. K. Ridley, Quantum Processes in Semiconductors, Clarendon Press, Oxford, Chapter 3, (1982)

[24] A. Kahan, M. Chi, and L. Friedman, J. Appl. Phys. **75**, 8012 (1994)

[25] G. Sun and L. Friedman, Superlattices and Microstructures **17**, No.3, (1995)

[26] B. K. Ridley, J. Phys. C: Solid State Phys. **15**, 5899 (1982)

[27] J. Bean, Proc. IEEE **80**, 571 (1992)

[28] J. Faist, F. Capasso, D. L. Sivco, A. L. Hutchinson, C. Sirtory, S. N. G. Chu, and A. Y. Cho, Appl. Phys. Lett. **65**, 2091 (1994)

[29] L. Friedman and R. A. Soref, IEEE Photonics Technology Letters **5**, 1200 (1993)

[30] L. J. Schowalter and R. W. Fathauer, CRC Critical Review **15**, 367 (1989)

[31] R. Tsu, Nature **364**, 19 (1993)

[32] M Yokoyama, K. I. Kashiro, and S. I. Ohta, J. Crystal Growth **81**, 73 (1987)

[33] X. Zhou, S. Jiang, and W. P. Kirk, J. Appl. Phys. **82**, 2251-2262 (1997)

[34] E. G. Wang and C. S. Ting, Phys. Rev. B **51**, 9791 (1995)

[35] C. Maierhofer, S. Kulkarni, M. Alonso, T. Reich, and K. Horn, J. Vac. Sci. Technol. B **9**, 2238 (1991)

[36] M. Cardona and N. E. Christensen, J. Vac. Sci. Technol. B **6**, 1285 (1988)

[37] W. A. Harrison, J. Vac. Sci. Technol. **14**, 1016 (1977)

[38] S. Jiang, X. Zhou, K. P. Clark, G. Spencer, R. T. Bate, W. P. Kirk, R. M. Steinhoff, and B. Brar (unpublished).

[39] A. Fasolino, E. Molinari, and J. C. Mann, Phys. Rev. B **39**, 3923 (1989)

[40] L. Friedman, R. A. Soref, and G. Sun, IEEE Photonics Technology Letters, **9**, 593 (1997)

[41] R. A. Soref, L. Friedman, L. C. Lew Yan Voon, L. R. Ram-Mohan, and G. Sun, submitted to J. Vac. Sci. Technol. B (to be published)